HYBRID MODELING OF HEAVY-ION COLLISIONS IN URQMD*

Marcus Bleicher, Bjørn Bäuchle, Stephan Endres
Thomas Lang, Gunnar Gräf

Institut für Theoretische Physik, Goethe Universität Frankfurt, Germany
and
Frankfurt Institute for Advanced Studies (FIAS), Frankfurt, Germany

(Received February 14, 2013)

We show a broad range of results from the Ultra-relativistic Quantum Molecular Dynamics (UrQMD) Boltzmann approach to relativistic heavy-ion collisions. The presented findings are calculated via Hybrid UrQMD with an intermediate hydrodynamic evolution. Results on photon emission, charmed mesons and dilepton production are shown.

DOI:10.5506/APhysPolBSupp.7.173
PACS numbers: 25.75.Cj, 24.10.Lx, 24.10.Nz

1. Introduction

Heavy-ion collisions offer the unique possibility to probe nuclear matter under extreme conditions experimentally and to study the properties of this matter systematically. To bring the nuclei up to relativistic energies, physicists use accelerators such as the Large Hadron Collider (LHC), the Relativistic Heavy-Ion Collider (RHIC) or the currently constructed FAIR facility. In these collisions, it is expected that a Quark–Gluon Plasma (QGP) is created in which quarks and gluons, which are subject to the strong force, can freely move around. The main goal of heavy-ion physics is to explore the strong force. The small size and the short time scale of the collisions prevents direct observation of the interaction medium. Only the fragments leaving the collision zone are observable. To get information about the medium evolution nevertheless, theoretical models like [1–5] are employed.

* Lecture presented by M. Bleicher at the XXXI Max Born Symposium and HIC for FAIR Workshop "Three Days of Critical Behaviour in Hot and Dense QCD", Wrocław, Poland, June 14–16, 2013.

A heavy-ion collision takes place in several, partially overlapping, stages. The initial stage consists of accelerated nuclei that behave already differently than just the sum of their nucleons. After this, the first hard interactions take place, the nucleons are stopped and new particles are produced. In the third stage, the medium is very dense which leads to a high interaction rate of particles. Often, this stage is assumed to be thermalized. At the end of the collision, the density, as well as the interaction rate, drops and particles cease to interact which is called freeze-out. At some point of the collision, hadronization takes place if the medium reached a deconfined state.

To explore the early stages of the collisions, probes that are sensitive to these early times or to the conditions during the whole evolution are needed. Such probes are discussed in the context of the UrQMD Hybrid model.

2. Hybrid approaches

The different stages of heavy-ion collisions are very different in their nature and are thus best described by different theoretical approaches. However, the ultimate goal is to describe the evolution of a collision from start to end within a single framework. To this aim, it was proposed [6, 7] nearly 15 years ago to combine hydrodynamic models, that are good at describing stages with a high interaction rate, with microscopic Boltzmann transport models, which are good describing matter with a low interaction rate. This class of models is often referred to as Hybrid models and they have been employed for a wide range of investigations [8–12]. The hybrid model used here is the UrQMD hybrid approach [13] (available for download [14]).

A hybrid event in UrQMD begins with UrQMD in cascade mode. First, the nuclei are initialized and are brought to collision. Once the nuclei with radius R have passed through each other, the hydrodynamic evolution starts at time $t_{\mathrm{start}} = 2R/\sqrt{\gamma^2 - 1}$. For this, the particles are mapped onto a hydrodynamic grid, explicitly assuming a local thermal equilibrium for each cell. The hydro evolution is performed using the SHASTA [15, 16] algorithm. After the energy density of all cells in a transverse slice of thickness 0.2 fm drops below five times nuclear groundstate density, the hydro degrees of freedom in this slice are mapped to particles using the Cooper–Frye equation [17]. This allows to treat the final state interactions in UrQMD cascade mode again.

3. Photons

Photons are an ideal probe to investigate the whole evolution of heavy-ion collisions. Once created, they leave the collision zone unperturbed due to their small interaction cross section. We use the UrQMD hybrid approach to disentangle the contributions from various phases of the heavy-ion collision to the photon spectra.

The small creation probability of direct photons allows us to calculate their emission perturbatively, so that the creation of direct photons does not alter the evolution of the underlying event.

Direct photon production in the model mostly comes from the channels $\pi\pi \to \gamma\rho$ and $\pi\rho \to \gamma\pi$ as well as from processes in the Quark–Gluon Plasma. The corresponding rates for hadronic photon emission from each hydrodynamic cell are taken from Turbide *et al.* [18], for the partonic emission the parameterizations from Arnold *et al.* [19]. In the transport part, the corresponding cross sections have been calculated by Kapusta *et al.* [20].

The cross sections from Kapusta and the rates from Turbide, although derived from different Lagrangians, have been found to be consistent with each other in previous investigations (see [21]). The numerical implementation for direct photon emission is explained in detail in [21].

At high transverse momenta, also prompt contributions from hard scatterings of partons in the initial nuclei become important. Gordon and Vogelsang [22] predicted the spectra by NLO-pQCD calculations. At high $p_\perp$

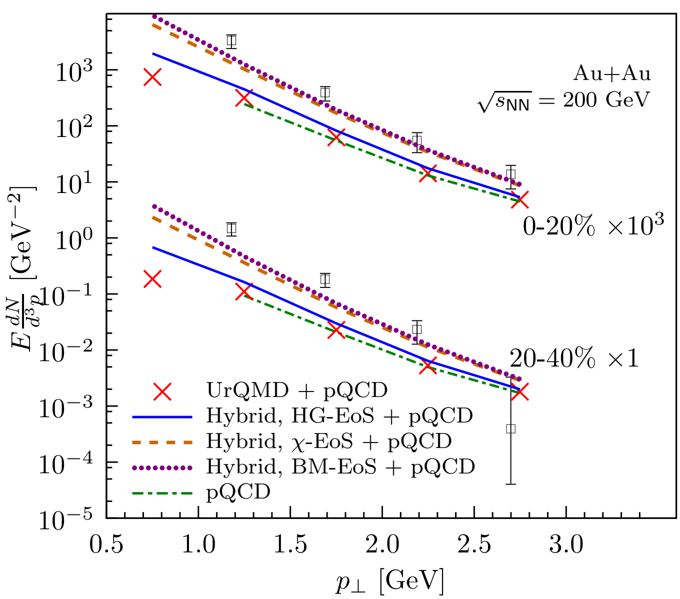

Fig. 1. (Color online) PHENIX Collaboration [26] data (black squares) on direct photons is compared to cascade calculations (red crosses) and hybrid calculations with HG-EoS (solid/blue lines), χ-EoS (dashed/orange lines) and BM-EoS (dotted/violet lines) for the 0–20% and 20–40% most central collisions. All spectra include the contributions from initial pQCD-scatterings [22, 26]. The spectra of the 0–20% most central collisions have been scaled by a factor of 10^3 for enhanced readability.

they fit the experimental data from the PHENIX Collaboration [23] rather well. For this reason, the pQCD contributions from [22] are scaled by the number of binary collisions and are added to the soft photons calculated here.

It has been pointed out by Fries *et al.* [24] and Qin *et al.* [25] that at intermediate transverse momentum jet-quenching and jet-medium interactions might increase the direct photon yield from hard pQCD processes. The effects of these processes are neglected in this analysis.

Figure 1 shows the comparison between direct photon $p_\perp$ spectra from cascade calculations and from PHENIX data [23] for Au+Au collisions at $\sqrt{s_{NN}} = 200$ GeV. The hadronic transport model results (solid lines) do not saturate the upper limits of the experimental data. The yield in all centrality bins is significantly larger than predicted by the hadronic cascade. However, the ratio of the hadronic and pQCD contributions is almost constant among the centrality bins. For comparison, the spectra obtained using the hybrid model with the Bag Model (BM-EoS) and with the chiral EoS (χ-EoS) are shown in Fig. 1. The agreement with data is good for both centralities.

4. Charmed mesons

FAIR will provide novel possibilities of probing strongly interacting matter [27], *e.g.* elliptic flow v_2 and the nuclear modification factor R_{AA} of charm quarks and D-mesons, at high net-baryon densities. Charm quarks are an excellent probe for heavy-ion collisions since they are produced in the beginning of collisions, live through the whole collision and carry information about the complete evolution of the system.

We explore the medium modification of heavy-flavor p_{T} spectra using the UrQMD hybrid model. The hydrodynamic phase is used as a background in which the heavy quarks are propagated by a relativistic Langevin approach. The drag and diffusion coefficients for the heavy-quark propagation in this framework are taken from a resonance approach [28, 29] where the existence of D-meson-like resonances in the QGP phase is assumed.

To account for the high baryon densities reached at FAIR energies, we implement an optional fugacity factor for our drag and diffusion coefficients. This fugacity factor leads to a stronger medium modification of $\overline{D}$- compared to D-mesons.

The space-time production coordinates of charm quarks in our approach are based on a space-time resolved Glauber approach.

The initial momentum distribution of the produced charm quarks at FAIR energy has not been measured so far. Therefore, we utilize a parametrization of HSD calculations [30] for the initial state of D- and $\overline{D}$-mesons.

Utilizing these initial conditions, we propagate the charm quarks on straight lines until t_{start}. For the Langevin calculation, we use the UrQMD hydro's cell velocities, cell temperature and the size of the time-step for the calculation of the momentum transfer, propagating all quarks independently. Once the system cools down, the charm quarks hadronize to D-mesons via quark-coalescence [31].

Our results for v_2 and R_{AA} are shown in Fig. 2. The highest elliptic flow can be seen for medium centralities of 20–40%. It reaches about half of the elliptic flow observed at RHIC and LHC energies. R_{AA} reaches the highest values for central collisions. Compared to higher energies the obtained values are extremely large. On the one hand, this is due to the soft initial charm spectra, on the other hand, it is due to a "heating up" of charm quarks in the medium.

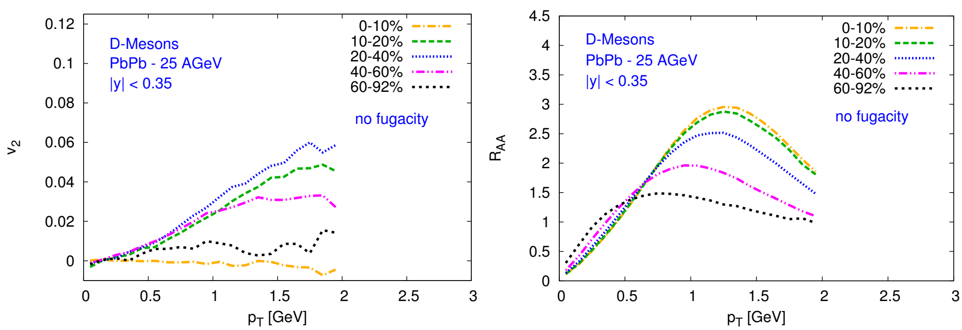

Fig. 2. (Color online) Elliptic flow v_2 (left) and nuclear modification factor R_{AA} (right) of D-mesons in Pb+Pb collisions at 25 AGeV for different centrality bins. We use a rapidity cut of $|y| < 0.35$. The different lines correspond to different collision centralities. The figures are taken from [32].

The calculations in Fig. 3 show the influence of including fugacity factors to account for the high baryo-chemical potential at FAIR energies on v_2 (left) and R_{AA} (right). A big difference for the results of D-mesons and $\bar{D}$-mesons can be seen. However, the difference between the calculation neglecting fugacity factors and the calculation for D-mesons including fugacity factors is small in the case of the elliptic flow. Here, the coalescence with light quarks accounts for the overwhelming fraction of the elliptic flow. The separate measurement of D-mesons and $\bar{D}$-mesons at FAIR energies can be an excellent test for the validity of the resonance model, since this difference cannot be seen in other models, *e.g.* in the T-Matrix approach [33].

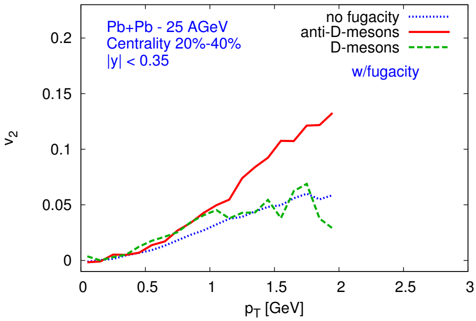

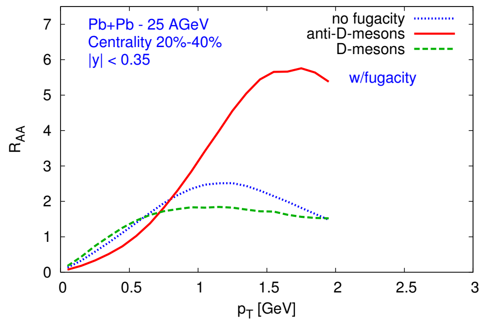

Fig. 3. (Color online) Elliptic flow v_2 (left) and nuclear modification factor R_{AA} (right) of D-mesons (dashed/green line) and $\overline{D}$-mesons (solid/red line) in Pb+Pb collisions at 25 AGeV applying fugacity factors. The dotted/blue line corresponds to a calculation without fugacity. We use a rapidity cut of $|y| < 0.35$. The figures are taken from [32].

5. Dimuons from a coarse-graining approach

The experimental observations of lepton pair production are successfully described using the UrQMD hybrid model. It was used in previous works to evaluate the thermal dilepton emission and the in-medium modifications of the ρ meson spectral function [34]. However, while this hybrid approach may give good results at SPS energies and above, the formation of a thermally equilibrated phase with fluid properties becomes questionable when going to the lower end of FAIR energies. On the other hand, the non-equilibrium treatment of in-medium effects (as off-shell effects and multi-particle scattering), which one expects during the hot and dense stage of heavy-ion collisions, is highly non-trivial in microscopic transport calculations. We, therefore, apply a different approach that uses the output from UrQMD calculations to extract local thermodynamic properties. This allows for the use of in-medium spectral functions and — via vector meson dominance — the calculation of thermal dilepton radiation. This ansatz has the advantage that it can be used even at energies and densities where hydro is no longer applicable.

For our calculations, we put a grid of space-time cells over an ensemble of several hundred UrQMD events, so that we get an average value of energy density ϵ and baryon density n_{B} in a small volume for each time step. The volume of the cells is chosen to be 1 fm^3 and the time resolution ranges from 0.5 to 1 fm, depending on the collision energy. According to Eckart's definition of the local rest frame the baryon four-flow $\vec{j}_{\mathrm{B}}$ is calculated and a Lorentz boost is performed so that the condition $\vec{j}_{\mathrm{B}} = 0$ is fulfilled.

To determine the dilepton production, we assume that every cell is in a thermally equilibrated state. However, as our approach shall cover the whole collision dynamics, one has to take into account that at the very beginning of the reaction the system is still far from a thermalized state. So even for the case of vanishing baryon flow, we might not find the energy momentum tensor to be diagonal. In this case, we apply a description that takes the momentum-space anisotropies into account [35]. For the corresponding space-time cells, we assume that the energy-momentum tensor takes the form

$$T^{\mu\nu} = (\epsilon + P_{\perp})U^{\mu}U^{\nu} - P_{\perp}g^{\mu\nu} - \left(P_{\perp} - P_{\parallel}\right)V^{\mu}V^{\nu} \tag{1}$$

with $P_{\perp,\parallel}$ being the transverse and longitudinal pressure respectively. $g^{\mu\nu}$ is the metric tensor, U^{μ} the flow velocity and V^{μ} the beam velocity vector. Once we know ϵ and n_{B} for each cell, temperature and baryon chemical potential can be determined by the use of a tabulated equation of state. For the SPS calculations, use a chiral EoS that incorporates a deconfinement phase transition and chiral symmetry restoration [36]. For lower bombarding energies, *e.g.* for SIS energies, we use a pure hadron gas EoS [37].

The strongest impact on thermal lepton pair production in the medium is expected to stem from the ρ meson contribution. The corresponding thermal emission rates per four-volume and four-momentum are in relation to the imaginary part of the ρ propagator D_{ρ}

$$\frac{d^8 N_{\rho\to ll}}{d^4x d^4q} = -\frac{\alpha^2 m_{\rho}^4}{\pi^3 g_{\rho}^2}\frac{L\left(M^2\right)}{M^2} f_{\mathrm{B}}(q_0;T)\,\mathrm{Im}\,D_{\rho}(M,q;T,\mu_B)\,, \tag{2}$$

where M is the muon pair invariant mass, f_{B} the Bose distribution and $L(M^2)$ the dimuon production phase space factor. The spectral function we apply in this case is the description by Eletsky *et al.* [38]. It is an empirical approach that includes the interaction with the constituents of the medium (*i.e.* the pions and nucleons) into the calculation of the ρ self energy.

At SPS energies and above, it is also necessary to include thermal contributions from the Quark–Gluon Plasma and from 4 pion interactions, as these sources here dominate the dilepton spectrum in the intermediate mass region above 1 GeV [39, 40].

In this section, we investigate two different scenarios. On the one hand, we make calculations for the NA60 dimuon measurement in In+In collisions at $E_{\mathrm{lab}} = 158$ AGeV and compare our results with the experimental data [41]. Secondly, we investigate Au+Au collisions at a low bombarding energy of 1.25 AGeV. The latter experiment has recently been carried out by the HADES Collaboration at GSI, however, the results are still pending. A previous study [42] shows a reasonable time evolution of the medium in this approach.

The resulting dilepton invariant mass spectra shown in Fig. 4 exhibit some interesting features. On the left-hand side, we see that the peak structure in the ρ contribution vanishes completely and the whole e^+e^- spectrum obtains a Dalitz type shape for the central Au+Au collisions at 1.25 AGeV. In the region below the pole mass, this leads to an enhancement of the total yield if compared to the result with a vacuum spectral function. This is mainly due to the sub-threshold contributions from the interactions with the Δ_{1232} and N^*_{1520} resonances, that are included in the spectral function. In the right plot, we compare our results with the dimuon excess data for In+In collisions at 158 AGeV. Also here, we see that the implementation of an in-medium ρ spectral function leads to higher dilepton production in the low mass-tail, in contrast to a pure vacuum ρ that exhibits a clear peak structure around the pole mass. However, we still underestimate the yield in the invariant mass region between 0.2 and 0.6 GeV. It is an interesting question for further studies whether the application of a different EoS and/or ρ spectral function (*e.g.* the approach by Rapp *et al.* [43]) might lead to a better agreement with experiment.

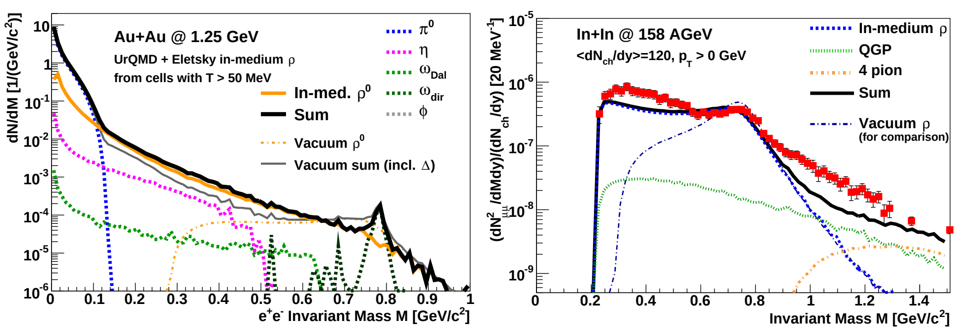

Fig. 4. (Color online) (Left) e^+e^- invariant mass spectrum for central Au+Au collisions with $E_{\text{lab}} = 1.25$ AGeV. The thermal contribution of the in-medium modified ρ, gained by coarse-graining, is shown together with the pure transport results for the other direct or Dalitz decays. (Right) Dimuon excess spectrum from coarse-grained dynamics for In+In at $E_{\text{lab}} = 158$ AGeV with $b < 9$ fm, compared to the experimental data from NA60 [41] (squares/red).

6. Summary

We have shown results on photon emission, charmed mesons and dimuons using the UrQMD hybrid model or in the case of the muons thermal emission from a microscopic evolution. All of the results rely on the combination of a microscopic non-equilibrium model with a macroscopic locally thermalized description.

In the case of the photons the hybrid treatment allows to disentangle the hadronic and the QGP contributions without running into the problems of microscopic hadronization. We have shown that most of the photons are emitted from the QGP phase.

The hybrid model is also very useful for describing D-meson production. The charm quarks are produced in the initial hard collisions that cannot be described in hydro, but in microscopic models. On the other hand, the hydro phase provides a more realistic modeling of the collective effects of the medium. This has also a big influence on the D-meson flow. All this allowed us to calculate the v_2 and R_{AA} centrality dependence of D-mesons. We found that a separate measurement of D- and $\overline{D}$-mesons can distinguish between the resonance model and the T-Matrix approach for the description of D-mesons in the medium.

The calculation of the dimuon spectra uses a different type of hybrid model where the evolution is treated completely microscopic, but in-medium effects are treated by calculating macroscopic quantities of the medium. As before, this facilitates the treatment compared to completely microscopic calculations. We find that the description of the experimental data is improved by taking into account the in-medium properties of the ρ meson.

REFERENCES

[1] Z.-W. Lin *et al.*, *Phys. Rev.* **C72**, 064901 (2005).

[2] K. Werner, F.-M. Liu, T. Pierog, *Phys. Rev.* **C74**, 044902 (2006).

[3] W. Cassing, E.L. Bratkovskaya, *Phys. Rev.* **C78**, 034919 (2008).

[4] Z. Xu, C. Greiner, *Phys. Rev.* **C71**, 064901 (2005).

[5] S.A. Bass *et al.*, *Prog. Part. Nucl. Phys.* **41**, 255 (1998).

[6] A. Dumitru *et al.*, *Phys. Lett.* **B460**, 411 (1999).

[7] S.A. Bass *et al.*, *Phys. Rev.* **C60**, 021902 (1999).

[8] O. Socolowski Jr. *et al.*, *Phys. Rev. Lett.* **93**, 182301 (2004).

[9] D. Teaney, J. Lauret, E.V. Shuryak, *Phys. Rev. Lett.* **86**, 4783 (2001) [arXiv:nucl-th/0110037].

[10] C. Nonaka, S.A. Bass, *Nucl. Phys.* **A774**, 873 (2006).

[11] T. Hirano, M. Gyulassy, *Nucl. Phys.* **A769**, 71 (2006).

[12] S. Ryu *et al.*, *Nucl. Phys.* **A904–905**, 389c (2013).

[13] H. Petersen, M. Bleicher, S.A. Bass, H. Stocker, arXiv:0805.0567 [hep-ph].

[14] UrQMD Homepage, http://www.urqmd.org

[15] D.H. Rischke, S. Bernard, J.A. Maruhn, *Nucl. Phys.* **A595**, 346 (1995).

[16] D.H. Rischke, Y. Pursun, J.A. Maruhn, *Nucl. Phys.* **A595**, 383 (1995) [*Erratum ibid.* **A596**, 717 (1996)].

[17] F. Cooper, G. Frye, *Phys. Rev.* **D10**, 186 (1974).

[18] S. Turbide, R. Rapp, C. Gale, *Phys. Rev.* **C69**, 014903 (2004).

[19] P.B. Arnold, G.D. Moore, L.G. Yaffe, *J. High Energy Phys.* **0112**, 009 (2001).

[20] J.I. Kapusta, P. Lichard, D. Seibert, *Phys. Rev.* **D44**, 2774 (1991) [*Erratum ibid.,* **D47**, 4171 (1993)].

[21] B. Baeuchle, M. Bleicher, *Phys. Rev.* **C81**, 044904 (2010).

[22] L.E. Gordon, W. Vogelsang, *Phys. Rev.* **D48**, 3136 (1993).

[23] S.S. Adler *et al.* [PHENIX Collaboration], *Phys. Rev. Lett.* **94**, 232301 (2005).

[24] R.J. Fries, B. Muller, D.K. Srivastava, *Phys. Rev. Lett.* **90**, 132301 (2003).

[25] G.-Y. Qin *et al.*, *Phys. Rev.* **C80**, 054909 (2009).

[26] A. Adare *et al.* [PHENIX Collaboration], *Phys. Rev. Lett.* **104**, 132301 (2010).

[27] B. Friman *et al.*, *Lect. Notes Phys.* **814**, 1 (2011).

[28] H. van Hees, R. Rapp, *Phys. Rev.* **C71**, 034907 (2005).

[29] H. van Hees, V. Greco, R. Rapp, *Phys. Rev.* **C73**, 034913 (2006).

[30] W. Cassing *et al.*, *Nucl. Phys.* **A691**, 753 (2001).

[31] T. Lang, H. van Hees, J. Steinheimer, M. Bleicher, `arXiv:1211.6912 [hep-ph]`.

[32] T. Lang, H. van Hees, J. Steinheimer, M. Bleicher, `arXiv:1305.1797 [hep-ph]`.

[33] H. van Hees *et al.*, *Phys. Rev. Lett.* **100**, 192301 (2008).

[34] E. Santini *et al.*, *Phys. Rev.* **C84**, 014901 (2011).

[35] W. Florkowski *et al.*, *Nucl. Phys.* **A904–905**, 803c (2013).

[36] J. Steinheimer, S. Schramm, H. Stocker, *J. Phys. G* **38**, 035001 (2011).

[37] D. Zschiesche *et al.*, *Phys. Lett.* **B547**, 7 (2002).

[38] V.L. Eletsky *et al.*, *Phys. Rev.* **C64**, 035202 (2001).

[39] J. Cleymans, J. Fingberg, K. Redlich, *Phys. Rev.* **D35**, 2153 (1987).

[40] Z. Huang, *Phys. Lett.* **B361**, 131 (1995).

[41] R. Arnaldi *et al.* [NA60 Collaboration], *Eur. Phys. J.* **C61**, 711 (2009).

[42] S. Endres, H. van Hees, M. Bleicher, *PoS* **CPOD 2013**, 052 (2013).

[43] R. Rapp, G. Chanfray, J. Wambach, *Nucl. Phys.* **A617**, 472 (1997).